J. Chil. Chem. Soc., 58, Nº 4 (2013)

ONE POT SOLVOTHERMAL SYNTHESIS OF ORGANIC ACID COATED MAGNETIC IRON OXIDE NANOPARTICLES

VERÓNICA PAREDES-GARCÍA[1,2], NÉSTOR TOLEDO[2], JULIANO DENARDIN[2,3], DIEGO VENEGAS-YAZIGI[2,4], CARLOS CRUZ[2,5], EVGENIA SPODINE[2,5], ZHIPING LUO[6,7]*

[1] *Universidad Andres Bello, Departamento de Ciencias Químicas, Chile.*
[2] *CEDENNA, Chile*
[3] *Facultad de Ciencia, Universidad de Santiago de Chile, Chile*
[4] *Facultad de Química y Biología, Universidad de Santiago de Chile, Chile*
[5] *Facultad de Ciencias Químicas y Farmacéuticas, Universidad de Chile, Chile*
[6] *Microscopy and Imaging Center and Materials Science and Engineering Program, Texas A&M University, College Station, TX 77843, USA*
[7] *Department of Chemistry and Physics, Fayetteville State University, Fayetteville, NC 28301, USA*
(Received: July 19, 2013 - Accepted: November 19, 2013)

ABSTRACT

In this work we present the synthesis and characterization of iron oxide nanoparticles (IONPs), which were structurally and magnetically characterized. The use of iron salts and an organic acid (l-serine or ascorbic acid) as precursors under solvothermal conditions yielded these coated IONPs. The powder X-ray diffraction pattern of FeO-1 and FeO-2 is consistent with hematite (α-Fe_2O_3) and hematite-maghemite ((α-Fe_2O_3/γ-Fe_2O_3) respectively. The TEM analysis permits to estimate an average size of 10 nm for the FeO-1 sample. The magnetic characterization of the samples through the *M*(*H*) plots showed a very low coercivity value for both samples, being 53 Oe for FeO-1 and 10 Oe for FeO-2, indicating the very weak ferromagnetic character of the synthesized iron oxide species. Even though both organic acids under solvothermal conditions permit to obtain coated IONPs in one pot reaction, l-serine produces a more narrow-size distribution.

Keywords: Iron oxide, nanoparticles, hematite, maghemite, solvothermal synthesis, magnetism

INTRODUCTION

Nanoparticles (NPs), correspond to organic or inorganic submicron moieties that usually have novel properties compared with the bulk material [1]. Within the inorganic nanoparticles it is possible to find the magnetic NPs, which are characterized by the presence of unusual magnetic properties. High coercivity, low Curie temperature, high magnetic susceptibility or superparamagnetism is characteristics of the magnetic NPs [2].

The interest to synthesize and study the magnetic NPs is due to a wide variety of applications in fields such as magnetic fluids, data storage, catalysis, biology and medicine, among others [3]. For example, the use of these type of nanoparticles in magnetic ferrofluids and data storage has allowed innumerable commercial applications [2,4]. Currently, the magnetic nanoparticles are being studied primarily due to the potential applications in biology and biomedicine. Targeted drug delivery, magnetic fluid hyperthermia (MFH), magnetic resonance imaging (MRI), magnetic bioseparations are some examples, where the magnetic NPs are being applied [5]. However, the choice of the magnetic nonmaterial depends on which type of application is desired. For instance, magnetically hard NPs are desirable for data storage, while all biological and biomedical applications require NPs which are biocompatible, non-toxic and chemically stable [5a,b-6].

Iron oxide nanoparticles (IONPs) belong to a special class of magnetic nanoparticles, which have been widely studied due to their scientific and industrial applications, which can range from data storage to MRI. There are different types of iron oxides, such as wustite (FeO), mixed iron (II, III) oxide (Fe_3O_4, magnetite), and iron (III) oxides, including alpha phase ((α-Fe_2O_3, hematite), beta phase (β-Fe_2O_3), gamma phase (γ-Fe_2O_3, maghemite), and epsilon phase (ε-Fe_2O_3) [7].

Many synthetic methods have been used to obtain magnetic iron oxide nanoparticles. These include organic solvent heating method, polyol method, and co-precipitation method [2,8]. Furthermore, several biological compounds have been used as surface coatings to prevent the aggregation of the NPs, for control size and biocompatibility [8]. However, the biomedical and bioengineering applications of the superparamagnetic iron oxide nanoparticles (SPIONs) are limited by the magnetic properties and size of these NPs. SPIONs having high magnetization values, size smaller than 100 nm, and an overall narrow particle size distribution, are very attractive due to the fact that they present uniform physical and chemical properties [9]. Beyond the magnetic applications, magnetite and hematite have also been used as catalysts for a number of industrially important reactions such as the Haber process (synthesis of NH_3), desulfurization of natural gas, dehydrogenation of ethyl benzene to styrene, the Fisher-Tropsch synthesis for hydrocarbons, oxidation of alcohols, and others [3e-i]. Besides, the three forms of magnetic iron oxide are used in synthetic pigments in paints, ceramics, and porcelain. However, the utility and therefore the applications of the iron oxides depend on the particle size and shape, size distribution, surface chemistry, degree of structural defects or impurities present in the particles, which can be related to the used synthetic procedure [3j-l].

Because of these extensive technological and industrial applications of the different iron oxide compounds, finding new synthetic routes to obtain this class of oxides is very motivating. In this work, we inform the synthesis and characterization of two types of iron oxides magnetic nanoparticles (FeO-1 and FeO-2), which were obtained by solvothermal synthesis from Fe^{III} salts and organic acids, as reagents. In both types of nanoparticles, in addition to the iron oxides, the presence of coating of the NPs by the organic reagent was also detected. Finally, both samples were structural and magnetically characterized.

EXPERIMENTAL

All starting materials were commercially available reagents with analytical grade, which were used without further purification. The iron oxides (FeO-1) and (FeO-2) were obtained by solvothermal synthesis in DMF in a 23 mL Teflon-lined stainless steel autoclave heated at 170 ºC for 24 h under self-generated pressure. After slow cooling (0.05 ºC/min) at room temperature the solid product was filtered off and dried at 40 ºC. The reagents used to obtain FeO-1 were 2-amino-3-hydroxypropanoic acid (l-serine), $FeCl_3{\cdot}4H_2O$ and Na_3PO_4 in a molar ratio of 1: 2: 0.65. FeO-2 was prepared using ascorbic acid, $FeCl_3{\cdot}4H_2O$, and K_2CO_3, in a molar ratio of 1: 2: 0.65. In both cases 5 mL of DMF were used as reaction solvent. Energy dispersive X-ray spectroscopy (EDXS) analyses performed on microcrystalline samples of FeO-1 and FeO-2, showed the presence of some type of iron oxide. Furthermore, both samples were analyzed by elemental analysis of carbon, obtaining a value of 1.1 and 6.0 % for FeO-1 and FeO-2 respectively.

X-Ray Powder Diffraction. Compounds FeO-1 and FeO-2 were analyzed by powder X-ray diffraction using a Siemens D5000 equipment, with Cu-$K\alpha_1$ radiation and Bragg-Brentano geometry in the $5^o \leq 2q \geq 80^o$ range. The analyses were performed using directly the microcrystalline samples. **Electron Microscopy and X-ray Spectroscopy.** Transmission electron microscopy (TEM) was done using a JEOL 2010 to determine the morphology, crystal structure and size distribution of the iron oxide nanoparticles. In order to make accurate size measurement, the magnifications were calibrated using SiC lattice fringes [10]. **FTIR and DRIFT Spectroscopy**. Absorption infrared and diffuse reflectance infrared spectra were recorded at room temperature on a Perkin Elmer Spectrum BX spectrophotometer. The infrared spectra were recorded

e-mail: vparedes@unab.cl

in the 4000–400 cm^{-1} range using KBr pellets. DRIFT spectra were obtained between 4000-400 cm^{-1} on solid samples, in order to determine the presence of organic coating on the iron oxide compounds.

Magnetic Characterization. The magnetization curves of the synthesized iron oxide nanoparticles were recorded at room temperature on a vibrating sample magnetometer (VSM).

RESULTS AND DISCUSSION

Synthesis and X-Ray Powder Diffraction

The X-ray powder diffraction data of FeO-1 presents peaks at 2θ of 32.8, 35.6, 40.5, 49.3, 54.0, 62.4 and 63.7° (Figure 1a). These diffraction peaks with low intensity can be indexed with the planes (104), (110), (113), (024), (116), (214) and (300), respectively, corresponding to the rhombohedral phase of hematite (α-Fe_2O_3) [11]. Hematite is characterized by having a rhombohedrally centered hexagonal structure of the corundum type, with a close-packed oxygen lattice in which two-thirds of the octahedral sites are occupied by Fe^{III} ions. The space group is $R\bar{3}c$ and the lattice parameters are a = 5.0356Å, c = 13.7489 Å (JCPDS No. 79-0007) [12].

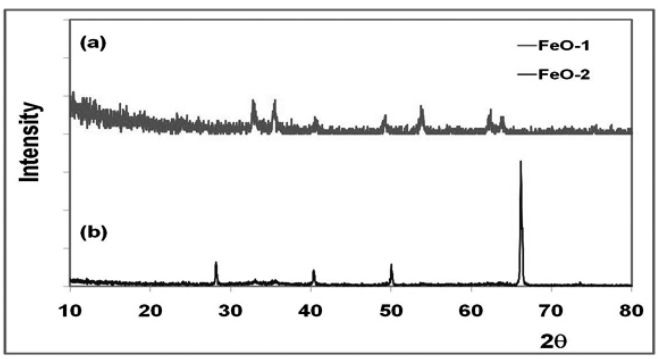

Figure 1. (a) Powder X-ray diffraction pattern of FeO-1. (b) Powder X-ray diffraction pattern of FeO-2.

The X-ray powder diffraction data obtained for FeO-2 permit to identify the presence of at least two components. One of them, presents peak at 32.6 and 35.5° which can be related with the (104) and (110) planes of α-F_2O_3 (Figure 1b). The very low intensity of the peaks can be due to the low crystallinity of the synthesized hematite (FeO-2). On the other hand, well-defined peaks at 2θ of 28.2, 39.9, 49.5, and 66.3° can be related to the presence of other crystalline iron oxides, such as maghemite (γ-Fe_2O_3) or magnetite (Fe_3O_4). Since both maghemite and magnetite have cubic spinel structure, the XRD patterns of these iron oxides are very much alike, and then the differentiation of these two phases using XRD is not straightforward [13].

γ-Fe_2O_3 is an allotropic form of Fe_3O_4, that is, these two iron oxides are crystallographic isomorphous. The main difference between these iron oxides is the presence of Fe^{II} and Fe^{III} ions in Fe_3O_4, while only Fe^{III} ions exist in γ-Fe_2O_3. Magnetite has the ferric ions distributed equally between the tetrahedral and octahedral sites, whose unit cell can be represented as $(Fe^{3+})_8[Fe^{2.5+}]_{16}O_{32}$, while maghemite as $(Fe^{3+})_8[Fe^{3+}_{5/6}\ \square_{1/6}]_{16}O_{32}$, where the brackets () and [] designate tetrahedral and octahedral sites, respectively [13c,d]. The X-ray diffraction pattern of maghemite possesses additional weak lines, which are attributed to vacancy ordering on the octahedral site. However, due to the lower intensities of these additional peaks, they are not used to differentiate magnetite from maghemite [13].

The presence of hematite as final product in FeO-1 and FeO-2 solids is not unusual if it is considered that hematite is the thermally most stable polymorph of all $iron^{III}$ oxides, which can be obtained by the thermal conversion of a wide variety of $iron^{II}$ and $iron^{III}$ compounds. For example, it can be prepared from ferric salts in strongly acidic media, or by decomposition of iron chelates in alkaline media [12].

To measure the particle size, the first approach used was the Scherrer formula (equation 1):

$$D = \frac{0.9\lambda}{\beta \cos\theta} \qquad (1)$$

where, D corresponds to the mean size, λ is the X-ray wavelength, β is the line broadening at half the maximum intensity and θ is the Bragg angle. The accuracy of the mean size value obtained by this method is dependent of the peak width. Therefore, a good resolution of the X-ray powder diffractogram is significant to obtain the particle size. Consequently, the shape of the crystal and size distribution, and/or the Debye thermal broadening due to vibrations of the lattice, also strongly affects the precision of the size particle values [14].

Based on the (104) peak of FeO-1 and taking into account the poor resolution of the diffractogram, the mean size obtained from equation (1) was 13.1 nm. This value is close to the value found by electron microscopy. In the case of FeO-2, the diffractogram presents a very good resolution for the peaks at 28.2, 39.9 and 49.5°, being the most intense peak the one at 28.2°. Using this peak to estimate the size of the particle, the obtained value for the size is 75.7 nm.

Infrared and Diffuse Reflectance Infrared Spectroscopy

The infrared spectrum obtained for the solid sample of FeO-1 shows absorptions at 3400, 1615, 540 and 460 cm^{-1}. Very weak absorptions are also observed at 1368 and 1054 cm^{-1}. A similar band pattern was obtained for FeO-2 showing weak absorptions at 3380, 1604, 1354, 1052 and 580 cm^{-1} with shoulders at and 684 and 460 cm^{-1} (see Figure 2). For both samples the absorption in the low energy region (< 600 cm^{-1}) corresponds to Fe-O vibrations, and the high energy region should be associated to the presence of organic species and water molecules. It is important to note that a broadening of the bands at low wave number is observed for FeO-2. Literature data inform two absorptions for hematite at 440 and 526 cm^{-1}, corresponding to the E_u and A_{2u}+E_u vibration modes respectively [15]. However, Sreeram et al. have assigned the absorptions at 471 and 587 cm^{-1} as characteristic of the Fe-O stretching vibrations of crystalline hematite [9c]. Besides, similar absorptions near to 440 and 550 cm^{-1} have been assigned to the T_{1u} vibration modes of maghemite and magnetite with spinel crystal structure [15].

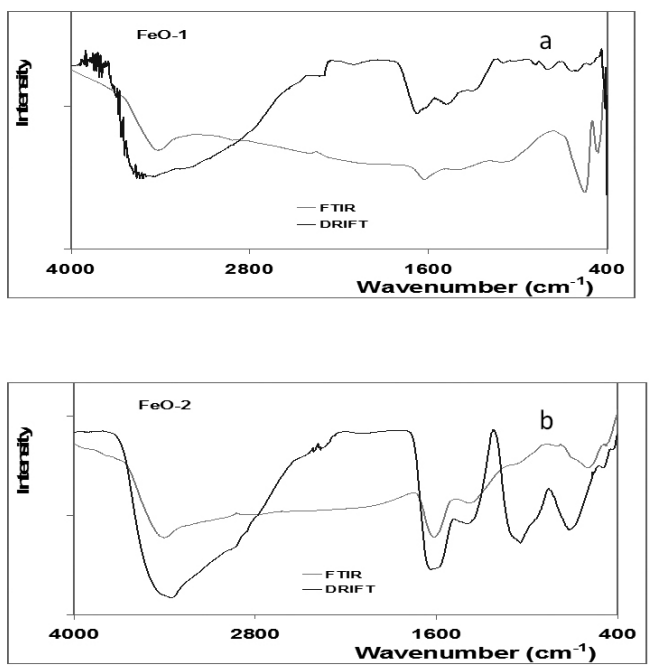

Figure 2. (a) Infrared (red line) and DRIFT (blue line) spectra of FeO-1. (b) Infrared (red line) and DRIFT (blue line) spectra of FeO-2.

According to literature data, the absorptions observed between 460 and 540 cm^{-1} in FeO-1, can be related with the E_u and A_{2u}+E_u hematite vibration modes, respectively. In the case of FeO-2, the broadening of the band centered at 580 cm^{-1} can be attributed to the mixture of iron oxides present in this sample. This absorption, together with the shoulder observed at 460 cm^{-1} should be related with the characteristic T_{1u} vibration modes of spinel type iron oxides, such as maghemite and magnetite.

On the other hand, the bands around 1100 cm^{-1} can be assigned to the symmetric stretching vibration of the C–O bond, which is present in both

organic molecules (serine and ascorbic acid) used as reagents to obtain the FeO-1 and FeO-2 iron oxide particles [9c]. The absorptions at 3500 and 1650 cm^{-1} are attributed to the water molecules adsorbed on the surface of FeO-1 and FeO-2 [16].

The DRIFT spectra of FeO-1 and FeO-2 are also given in figure 2. The presence of organic species, together to the synthesized iron oxide nanoparticles, is also evidenced by the absorption pattern obtained for both samples. Wide absorptions at approximately 3400, 1640, 1450, 1100 and 750 cm^{-1} are observed. The bands at 1660 and 1450 cm^{-1} can be assigned to carboxylate groups [17].

The use of diffuse reflectance spectroscopy has allowed to identify the presence of organic compounds in the samples, which correspond to serine in the case of compound FeO-1, and ascorbic acid in the case of FeO-2. Therefore, the presence of these organic absorptions is strong evidence that the organic compounds are covering the iron oxide nanoparticle surface.

Electron Microscopy

The morphology and size of the particles were analyzed by electron microscopy techniques. Representative SEM and TEM images of FeO-1 at different magnification are shown in Figure 3. Low magnification SEM image (see Figure 3a) shows circular plates of uniform size sorted in different directions, giving morphologies similar to flowers. This arrangement is lost when the SEM image is obtained at a higher magnification (see Figure 3b).

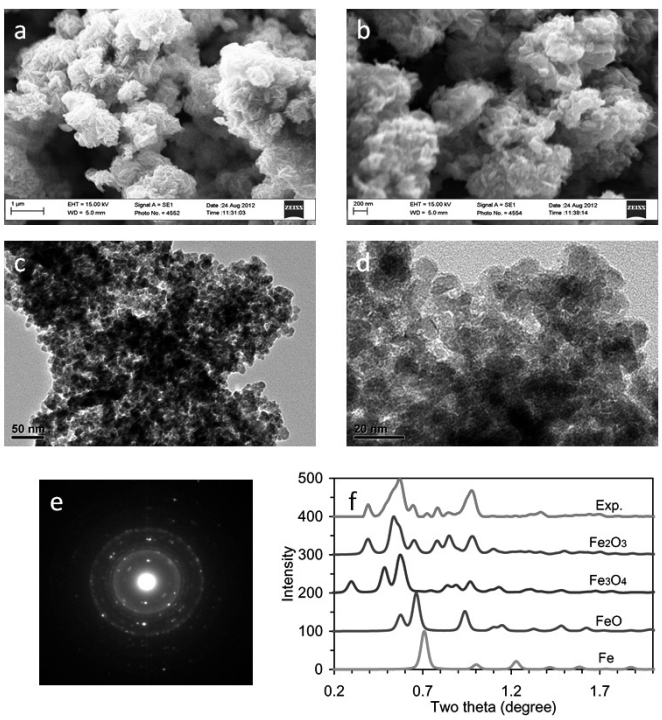

Figure 3. SEM and TEM images of FeO-1. (a) Overview SEM image in a low magnification; (b) Enlarged SEM image; (c) Overview TEM image in a low magnification; (d) Enlarged TEM image; (e) Electron diffraction pattern showing poly rings from iron oxide nanoparticles; (f) Electron diffraction pattern of different iron oxide samples.

At this resolution the solid (FeO-1) does not show a defined morphology. Higher magnifications were obtained through of TEM analysis. A representative TEM image of FeO-1 is shown in Figure 3c, which is magnified in Figure 3d. It is seen that these NPs have uniform and small size. The presence of nanocrystals of iron oxide nanoparticles in the sample is evidenced by the electron diffraction pattern in Figure 3(e), showing the existing high crystallinity. The intensity profile of the electron diffraction pattern is retrieved after removing the background in the way reported previously [18], as shown in Figure 3(f). As compared with the simulations using structural models of Fe_2O_3, Fe_3O_4, FeO and Fe, the experimental data are very consistent with the Fe_2O_3 structure. The size distribution given in Figure 4 corresponds to a size variation between 1.8 and 20 nm, with a mean value of 10.1 nm, and standard deviation of 3.2 nm, based on the measurement of 219 nanoparticles. The nanoparticle size is found to be in a narrow size range [19]. It is important to remark that the mean size obtained by the Scherrer formula (13.1 nm) is very close to that estimated by TEM microscopy (10.1 nm).

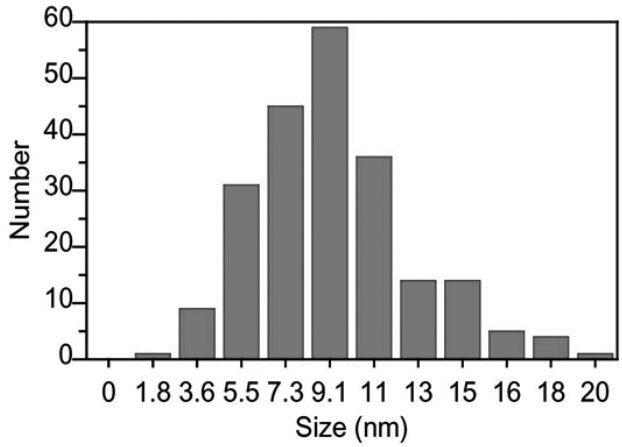

Figure 4. Size distribution of iron oxide nanoparticles in sample FeO-1.

The SEM and TEM images obtained for FeO-2 are given in Figure 5. Unlike the NPs of iron oxide of FeO-1, the SEM images obtained for FeO-2 (see Figure 5a and 5b) do not have small and uniform size, and also do not present a special morphology. Some agglomerates lower than 200 nm can be evidenced from the SEM image given in Figure 5b. It was impossible to determine the size distribution from the TEM image obtained for FeO-2 (see Figure 5c), because its low quality. Furthermore, a very low crystallinity of the sample of FeO-2 as compared with that of FeO-1 can be observed by the electron diffraction pattern given in Figure 5(d). Therefore, from the SEM and TEM data of FeO-2, it is only possible to infer that the average size of the NPs is significantly larger than that in FeO-1, which is consistent with the XRD results.

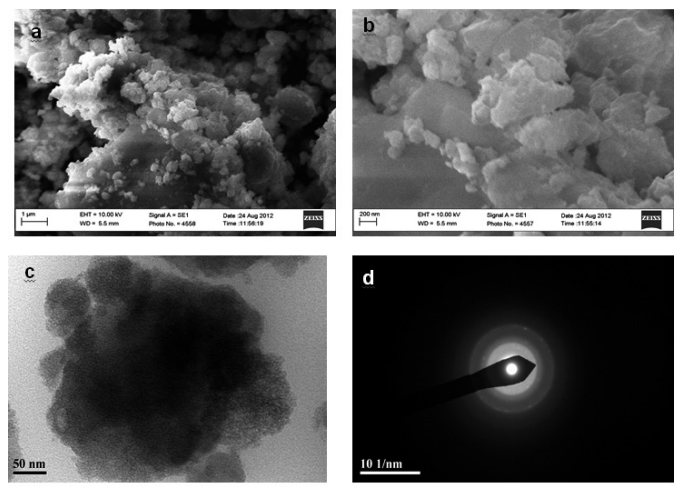

Figure 5. SEM and TEM images of FeO-2. (a) Overview SEM image in a low magnification; (b) Enlarged SEM image; (c) Overview TEM image in a low magnification; (e) Electron diffraction pattern of FeO-2 sample.

Magnetic Measurements

The magnetization curves of the synthesized iron oxide nanoparticles were measured at room temperature, under a maximum applied field of 10 kOe. Hysteresis loops $M(H)$ of FeO-1 and FeO-2 are shown in Figure 6.

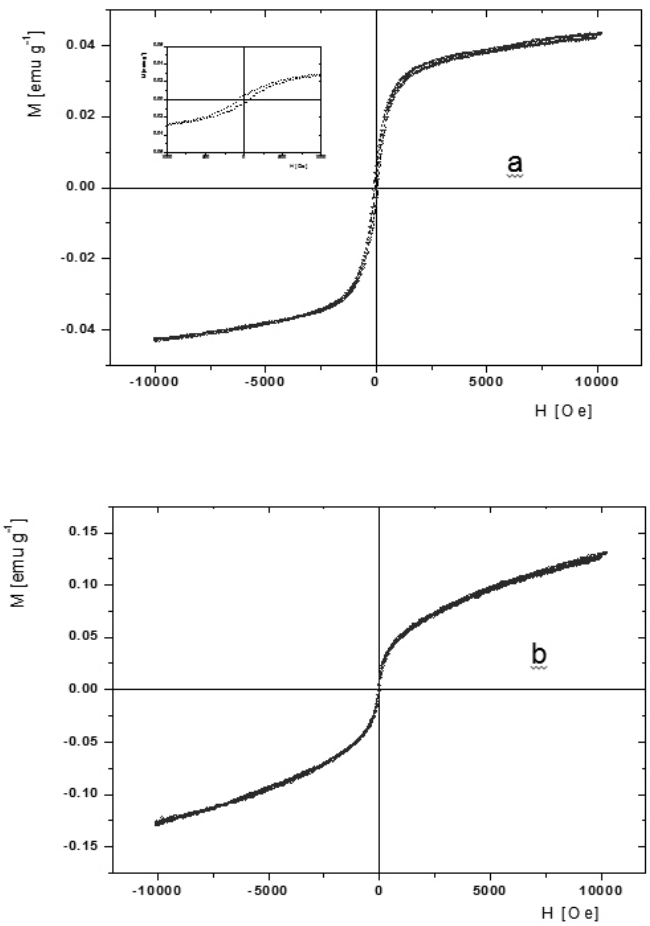

Figure 6. (a) Hysteresis loop of FeO-1. (b) Hysteresis loop of FeO-2.

Although a complete magnetic saturation is not achieved in either cases, the $M(H)$ plot obtained for FeO-1 shows that the magnetization of the sample is closer to the saturation value than that for FeO-2. For FeO-1, a fast increase of the magnetization is observed until 2.5 kOe and at higher field, the near saturation value obtained for FeO-1 was 0.04 emu g^{-1}. Hysteresis is observed for FeO-1, indicating the ferromagnetic behavior at room temperature. From the $M(H)$ plot it is possible to obtain values of coercivity (H_c) and a remanent magnetization (M_r) of 53 Oe and 0.005 emu g^{-1} respectively (inset Figure 6a). These values are in the order of the reported ones for analogous flower-like α-Fe_2O_3 [20].

The bulk hematite is classified as a weak ferromagnetic material at room temperature, presenting a weak magnetization. It is known that the particles of a ferromagnetic material change from a multidomain to a single domain, when the size of the magnetic particles decreases, thus causing the phenomenon of superparamagnetism [21]. Considering previous reports, the hematite critical size for the transition from ferromagnetic to superparamagnetic behavior, depends on the particles shape, the strain and defects in the particles induced by the different synthetic routes [22-24]. Thus, for spherical hematite, the reported biggest threshold diameter is about 41 nm, below this size the particles become superparamagnetic (Hc≈0) [25]. Nonetheless, for one dimensional nanostructures (hematite nanorods), the value is 15~25 nm in breadth and 170~330 nm in length. On the other hand, for larger particles of hematite the coercivity depends mainly on the grain size and the morphology. Svoboda et al. noted that depending on the microstructure of the hematite particles, the coercivity H_c may range from 0.3 to 3 kOe [26]. In the case of FeO-1, the coercivity value is much lower than the range reported by Svoboda. Therefore, supposing a multidomain structure for the synthesized hematite nanoparticles, which could explain the observed coercivity, does not appear as coherent if the average size of 10 nm is considered. Therefore, the fact that a non-complete magnetic saturation was observed at the maximum applied magnetic field, can be explained by the increase of the surface spin disorder, and the very small coercivity can be attributed to some magnetically blocked spins at room temperature [27].

The hysteresis loop for FeO-2 shows that the remanence and coercivity are very much lower than that observed for FeO-1 (M_r=0.004 $emug^{-1}$ and H_c=10 Oe). Even though the magnetization values are higher than those obtained for FeO-1 (M_s=0.13 emu g^{-1}). Taking into account that bulk maghemite and magnetite have a magnetic saturation of 80 and 92 emu g^{-1} at room temperature, respectively, and considering the M_s value obtained for FeO-2, it can be concluded that this synthesized iron oxide should be constituted mainly by α-Fe_2O_3. According with the complete experimental evidence of these synthesized IONPs we can conclude that the main constituent in both samples is hematite (α-Fe_2O_3), while the sample FeO-2 also could contain a minor amount of maghemite or magnetite. However, due to structural similarities between maghemite and magnetite and also by their spectroscopic and magnetic properties, the identification of the constituents in sample FeO-2 remains a challenge.

From a chemical point of view, the process for the preparation of some iron oxides starting from iron oxyhydroxide, which can be obtained from iron (III) salts is presented in the following scheme [13a,28]:

$$FeX_3 + 3H_2O + 3RNH_2 \longrightarrow Fe(OH)_3 + 3RNH_3X$$

$$Fe(OH)_3 \longrightarrow FeOOH$$

$$FeOOH \xrightarrow{\text{dehydratation}} \alpha\text{-}Fe_2O_3 \xrightarrow{\text{reduction}} Fe_3O_4 \xrightarrow{\text{oxidation}} \gamma\text{-}Fe_2O_3$$

In this chemical process, the magnetite appears as the first product obtained from hematite. However, in the solvothermal synthesis, redox processes can easily occur. Taking into account that hematite and maghemite correspond to the most frequent mixture of iron oxides present in nature, it is possible to infer that sample FeO-2 is composed of hematite and maghemite.

CONCLUSIONS

Synthesized hematite and a mixture of hematite and maghemite nanoparticles were obtained under solvothermal conditions. Both samples were characterized by powder X-ray diffraction, electronic microscopy and magnetic measurements. In both iron oxide samples the presence of an organic coating can be evidenced by diffuse reflectance FTIR spectroscopy. The magnetic characterization of the iron oxide nanoparticles shows that the hematite sample, FeO-1, presents a weak ferromagnetic behavior with a very low coercivity value. This is greater than the observed for the synthesized hematite-maghemite mixture, FeO-2. In both cases complete magnetization saturation is not achieved, indicating the increasing surface spin disorder in both synthesized iron oxides samples. Furthermore, the magnetization values obtained for FeO-2, suggests that the synthesized hematite is the main component in the sample.

ACKNOWLEDGMENTS

The authors acknowledge financial support from FONDECYT 1090477, DI-UNAB-104-12/R and Proyecto Basal CEDENNA, Financiamiento Basal FB0807.

REFERENCES

1. (a) L. LaConte, N. Nitin, G. Bao. Mater. Today. **8**, 32, (2005). (b) V. Balzani. Small. **1**, 278, (2005). (c) G Cárdenas-Triviño, O. Godoy-Guzmán, G. Conterreas. J. Chil. Chem. Soc. **54**, 6, (2009). (d) Y. León, I. Brito, G. Cárdenas, O. Godoy. *J. Chil. Chem. Soc*. **54**, 51, (2009).
2. (a) W. Wu, Q. He, Ch. Jiang. *Nanoscale Res. Lett*. **3**, 397, (2008). (b) S. Laurent, D. Forge, M. Port, A. Roch, C. Robic, L. V. Elst, R.N. Muller. *Chem. Rev*. **108**, 2064, (2008).
3. (a) L.A. Thomas, L. Dekker, M. Kallumadil, P. Southern, M. Wilson, S.P. Nair, Q.A. Pankhurst, I.P. Parkin. *J. Mater. Chem*. **19**, 6529, (2009). (b) J.S. Jiang, Z.F. Gan, Y. Yang, B. Du, M. Qian, P. Zhang. *J. Nanopart. Res*. **11**, 1321, (2009). (c) K. Chen, J. Xie, H. Xu, D. Behera, M.H. Michalski, S. Biswal, A. Wang, X. Chen. *Biomaterials*. **30**, 6912, (2009). (d) C. Altavilla, E. Ciliberto Inorganic Nanoparticles. Synthesis, Applications, and Perspectives. CRC Press, Taylor and Francis Group, USA, 2010. (e) A.S. Teja, P.-Y. Koh. Prog. Cryst. Growth Ch. **55**, 22, (2009). (f) Q. Liu, Z.M. Cui, Z. Ma, S.W. Bian, W.G. Song, L.J. Wan. *Nanotechnology*. **18**, 385605, (2007). (g) F. Shi, M.K. Tse, M.M. Pohl, A.

Brückner, S. Zhang, M. Beller, *Angew. Chem. Int. Edit*. **46**, 8866, (2007). (h) S. Al-Sayari, A.F. Carley, S.H. Taylor, G.J. Hutchings. *Top. Catal*. **44**, 123, (2007). (i) A.K. Kandalam, B. Chatterjee, S.N. Khanna, B.K. Rao, P. Jena, B.V. Reddy. *Surf. Sci*. **601**, 4873, (2007). (j) H. Gaedcke in Industrial Inorganic Pigments, G. Buxbaum ed. Wiley-VCH, Weinheim, 1998; pp. 181-188. (k) U.T. Lam, R. Mammucari, K. Suzuki, N.R. Foster. *Ind. Eng. Chem. Res*. **47**, 599, (2008). (l) R.M. Cornell, U. Schwertmann The Iron Oxides. Structure, Properties, Reactions, Occurrences and Uses, Wiley-VCH, Weinheim, 2003. (m) D. Ruiz, C. Mella, J.L.G. Fierro, P. Reyes. *J. Chil. Chem. Soc*. **57**, 1394, (2012).

4. N. Sounderya, Y. Zhang. Recent Patents on Biomedical Engineering **1**, 34, (2008).
5. (a) A. Figuerola, R. Di Corato, L. Manna, T. Pellegrino. *Pharmacol. Res*. **62**, 126, (2010). (b) J. Chomoucka, J. Drbohlavova, D. Huska, V. Adam, R. Kizek, J. Hubalek. *Pharmacol. Res*. **62**, 144, (2010). (c) A. K. Gupta, M. Gupta. *Biomaterials*. **26**, 3995, (2005). (d) P. Haddad, T.M. Martins, L. D`Souza-Li, L.M. Li, K. Metze, R.L. Adam, M. Knobel, D. Zanchet. *Mater. Sci. Eng. C*. **28**, 489, (2008).
6. (a) A. Millan, F. Palacio, A. Falqui, E. Snoeck, V. Serin, A. Bhattacharjee, V. Ksenofontov, P. Gutlich, I. Gilbert. *Acta Mater*. **55**, 2201, (2007). (b) G. Zhang, Y. Liao, I. Baker. *Mater. Sci. Eng. C-Mater Biol Appl*. **30**, 92, (2010). (c) J. Gao, H. Gu, B. Xu. *Acc. Chem. Res*. **42**, 1097, (2009). (d) N. L. Rosi, Ch. A. Mirkin. *Chem. Rev*. **105**, 1547, (2005). (e) R. Qiao, Ch. Yang, M. Gao. *J. Mater. Chem*. **19**, 6274, (2009).
7. (a) J. T. Nurmi, P.G. Tratnyek, V. Sarathy, D. R. Baer, J.E. Amonette, K. Pecher, Ch. Wang, J.C. Linehan, D.W. Matson, R.L. Penn, M. D. Driessen. *Environ. Sci. Technol.* **39**, 1221, (2005). (b) H. Karami. *J. Clust. Sci.* **21**, 11, (2010). (c) G. Zhen, B.W. Muir, B.A. Moffat, P. Harbour, K.S. Murray, B. Moubaraki, K. Suzuki, I. Madsen, N. Agron-Olshina, L.Waddington, P. Mulvaney, P.G. Hartley. *J. Phys. Chem. C*. **115**, 327, (2011). (d) C. Han, J. Xie, C. Deng, D. Zhao. *J. Chil. Chem. Soc*. **57**, 1372, (2012).
8. (a) J.P. Ge, Y.X. Hu, M. Biasini, C.L. Dong, J.H. Guo, W.P. Beyermann, Y.D. Yin. Chem. Eur. J. **13**, 7153, (2007). (b) T. Hyeon. *Chem. Commun.* 927, (2003). (c) Y. Wenguang, Z. Tonglai, Z. Jianguo, G. Jinyu, W. Ruifeng. *Prog. Chem*. **19**, 884, (2007). (d) Y.Y. Sun, G.Z. Guo, B.H. Yang, W. Cai, Y. Tian, M.H. He, Y.Q. Liu. *Physica B*. **406**, 1013, (2011).
9. (a) A.M. Schrand, M.F. Rahman,.S.M. Hussain, J.J. Schlager, D.A.Smith, A.F. Syed. WIREs Nanomed. *Nanobiotechnol*. **2**, 544, (2010). (b) D.A. Canelas, K.P. Herlihy, J.M. DeSimone. WIREs Nanomed. *Nanobiotechnol*. **1**, 391, (2009). (c) M. Nidhin, R. Indumathy, K.J. Sreeram, B.U. Nair. *Bull. Mater. Sci*. **31**, 93, (2008). (d) K.J. Sreeram, M. Nidhin, B.U. Nair. *Colloid Surface B*. **71**, 260, (2009). (e) M.P.S. de Almeida , K.L. Caiado, P.P.C. Sartoratto, D.O. Cintra, E. Silva , A.R. Pereira , P.C. Morais. *J. Alloy. Compd.* **500**, 149, (2010).
10. Z.P. Luo. *Acta Mater*. **54**, 47, (2006).
11. R.L. Blake, R.E, Hessevick, T. Zoltai, L.W. Finger. *Am. Mineral*. **51**, 123, (1966).
12. (a) H. Cao, G. Wang, L. Zhang, Y. Liang, S. Zhang, X. Zhang. *Chem. Phys*. **7**, 1897, (2006). (b) R.K Zboril, M. Mashlan, D. Petridis. *Chem. Mater*. **14**, 969, (2002).
13. (a) M. Gotic, G. Koščec, S. Music. *J. Mol. Struct*. **924-926**, 347, (2009). (b) X. Wang, X. Chen , X. Ma, H. Zheng, M. Ji,, Z. Zhang. *Chem. Phys. Lett*. **384**, 391, (2004). (c) R. Grau-Crespo, A.Y. Al-Baitai, I. Saadoune, N.H. De Leeuw. J. Phys-Condens. Mat. **22**, 255401, (2010). (d) K. Haneda, A. H. Morrish. *J. Phys. Colloques*. **38**, Cl-321, (1977).
14. V. Ciupină, S. Zamfirescu and G. Prodan in Evaluation of Mean Diameter values using Scherrer Equation Applied to Electron Diffraction Images, Nanotechnology- Toxicological Issues and Environmental Safety, P.P. Simeonova, N. Opopol, M.I. Luster eds. Springer, Netherlands, 2007; pp. 231-237.
15. (a) A.M. Jubb, H.C. Allen. ACS Appl. Mater. *Interfaces*. **2**, 2804, (2010). (b) S. Onari, T. Arai, K. Kudo. *Phys. Rev. B*. **16**, 1717, (1977). (c) C. J. Serna, J. L. Rendon, J.E. Iglesias. *Spectrochim. Acta, A*. **38**, 797, (1982).
16. R. Arbain, M. Othman, S. Palaniandy. *Miner. Eng*. **24**, 1, (2011).
17. I. F. Trotter, H.W. Thompson, F. Wokes. *Biochem. J.* **42**, 601, (1948).
18. Z.P. Luo, Y. Vasquez, J.F. Bondi, R.E. Schaak. *Ultramicroscopy* **111**, 1295, (2011).
19. Z.P. Luo. *J. Mater. Sci*. **45**, 3228, (2010).
20. S. Zeng, K. Tang, T. Li, Z. Liang, D. Wang, Y. Wang, Y. Qi, W. Zhou. *J. Phys. Chem. C*. **112**, 4836, (2008).
21. N. Amin, S. Arajs and E. Matijevic, *Phys. Status Solidi A*, **104**, K65, (1987).
22. T. P. Raming, A. J. A. Winnubst, C. M. van Kats, A. P. Philipse, *J. Colloid Interf. Sci.* **249**, 346, (2002).
23. F. Bodker, M. F. Hansen, C. B. Koch, K. Lefmann, S. Morup. *Phys. Rev. B*. **61**, 6826, (2000).
24. B. Tang, G. Wang, L. Zhuo, J. Ge, L. Cui. *Inorg. Chem*. **45**, 5196, (2006).
25. Z. Gan, A. Zhao, Q. Gao, M. Zhang, D. Wang, H. Guo,W. Tao, D. Li, E. Liu, R. Mao. *RSC Adv*. **2**, 8681, (2012).
26. J. Svoboda Magnetic Techniques for the Treatment of Materials, Springer, USA, 2004.
27. P.G. Bercoff, H.R. Bertorello. *Appl. Phys. A-Mater*. **100**, 1019, (2010).
28. Z. Li, X. Lai, H. Wang, D. Mao, C. Xing, D. Wang. *Nanotechnology*. **20**, 245603, (2009).